Nanoscale

Accepted Manuscript

This is an *Accepted Manuscript*, which has been through the RSC Publishing peer review process and has been accepted for publication.

Accepted Manuscripts are published online shortly after acceptance, which is prior to technical editing, formatting and proof reading. This free service from RSC Publishing allows authors to make their results available to the community, in citable form, before publication of the edited article. This *Accepted Manuscript* will be replaced by the edited and formatted *Advance Article* as soon as this is available.

To cite this manuscript please use its permanent Digital Object Identifier (DOI®), which is identical for all formats of publication.

More information about *Accepted Manuscripts* can be found in the **Information for Authors**.

Please note that technical editing may introduce minor changes to the text and/or graphics contained in the manuscript submitted by the author(s) which may alter content, and that the standard **Terms & Conditions** and the **ethical guidelines** that apply to the journal are still applicable. In no event shall the RSC be held responsible for any errors or omissions in these *Accepted Manuscript* manuscripts or any consequences arising from the use of any information contained in them.

Table of Contents

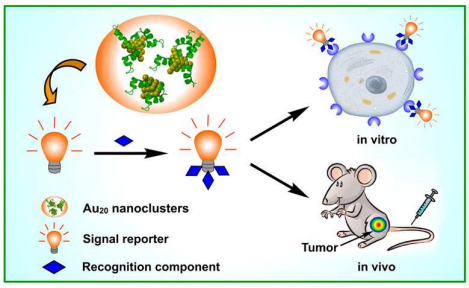

Receptor-mediated uptake of nanoprobes for tumor-targeting *in vitro* and *in vivo* is systematically studied using newly prepared luminescent Au_{20} nanoclusters.

Cite this: DOI: 10.1039/c0xx00000x

www.rsc.org/nanoscale

PAPER

Rapid Synthesis of Highly Luminescent and Stable Au_{20} Nanoclusters for Active Tumor-Targeted Imaging *in vitro* and *in vivo*

Pu Zhang,[a,c] Xiao Xi Yang,[b] Yi Wang,[b] Ning Wei Zhao,[d] Zu Hong Xiong,[c] and Cheng Zhi Huang*[a,b]

Received (in XXX, XXX) Xth XXXXXXXXX 20XX, Accepted Xth XXXXXXXXX 20XX
DOI: 10.1039/b000000x

Rapid synthesis of protein-stabilized Au_{20} nanoclusters (Au_{20}NCs) with high fluorescence quantum yield (QY) up to ~15% is successfully achieved by manipulating the reaction kinetics. The as-obtained Au_{20}NCs, identified by mass spectrometry, have an average size of 2.6 nm, with strong fluorescence emission at 620 nm (2.00 eV) either upon the excitation at 370 nm (3.35 eV) or 470 nm (2.64 eV). The advantages of the as-obtained Au_{20}NCs, including small sizes, high fluorescence QY, excellent photostability, non-toxicity, and good stability in biological media, make them be ideal candidates as good luminescent probes for optical imaging *in vitro* and *in vivo*. Our results demonstrate that the uptake of Au_{20}NCs by both cancer cells and tumor-bearing nude mice can be improved by receptor-mediated internalization, compared with that by passive targeting. Since being selectively accumulated at the tumor sites, the Au_{20}NCs probes can be used as a potential indicator for cancer diagnosis. This work not only provides a new understanding of the rapid synthesis of highly luminescent Au_{20}NCs but also demonstrates that the functionalized-Au_{20}NCs are excellent probes for active tumor-targeted imaging *in vitro* and *in vivo*.

1. Introduction

Fluorescence imaging is one of the most advanced techniques to achieve non-invasive and non-destructive visualization *in vivo*, and has attracted increasing attention in recent years due to its significant roles in biological and biomedical applications related to prognosis, diagnosis, and therapy of a variety of serious diseases.[1,2] Thus, rational design and synthesis of various fluorescent probes as signal reporters for fluorescence imaging is attractive. Since biological tissues can absorb and scatter photons and thus generate strong auto-fluorescence, collection and processing of fluorescence signal during the biological imaging are easy to be interfered, especially for the *in vivo* studies.[3,4] Thus, the probes with long wavelength emission from red visible region to near-infrared (NIR) region are highly favourable in bioimaging, because the living tissues are almost transparent within this range of wavelengths. To this end, a variety of different long wavelength fluorescent probes have been developed, including the traditional organic dyes, DNA beacons, fluorescent proteins, fluorescent conjugated polymers, semi-conducting quantum dots, silicon- and carbon-based nanomaterials, as well as the rising star of metal nanoclusters.[5-13]

Fluorescent gold nanoclusters (AuNCs), a member in the family of metal nanoclusters with the composition of tens to hundreds of Au atoms, stand out from various fluorescent probes due to their attractive features including subnanometer size, high fluorescence quantum yield (QY), excellent photostability and biocompatibility, and easy preparation. More importantly, AuNCs with tunable fluorescence emission (*e.g.*, from visible to NIR regions) can be achieved through controlling the reaction parameters and thus the number of Au atoms in a cluster.[14-26] To date, many strategies have been developed for the synthesis of AuNCs, including the chemical reduction, photochemical reduction, phase-transfer, chemical etching of metallic nanoparticles, and transformation from other metal nanoclusters *via* galvanic replacement reaction.[16-20] Among these approaches, chemical reduction in solution phase is the most favorable and general route for the preparation of AuNCs, in which a variety of different templates including dendrimers, polyelectrolytes, thiol-containing molecules, DNA, peptides, and proteins are available for the synthesis.[14-16, 21-26]

Proteins have been reported as excellent raw materials for the synthesis of AuNCs since they contain many active sites (*i.e.*, functional groups such as thiol, amino, hydroxyl, and carboxyl) to accumulate and reduce Au^{3+} ions, and can also stabilize the resultant AuNCs.[14-16] Although there have been many successful demonstrations for the synthesis of AuNCs with proteins, these methods are still troubled by issues such as relatively low fluorescence QY (usually lower than 6%) of the products [27-32] or time-consuming (generally, at least 12 h was required for a batch of synthesis) [29-38]. With regard to the applications of AuNCs, some reports have demonstrated that the fluorescence signal of their AuNCs can be used for optical imaging.[28-37] In addition, a few muti-functional nanoprobes such as Gd_2O_3/Au and Gd/Au

hybrids have also been fabricated recently, aiming to achieve the multimodal imaging. However, the uptake of the nanoprobes in most of these studies was based on the passive mode (*e.g.*, endocytosis).[36,37] In this case, the efficiency for the uptake of the optical probes would be relatively low, and the probes were also not be able to selectively accumulate at tumor sites. Taken together, better understanding of the mechanism for the synthesis of luminescent AuNCs and their performances in biological systems are still challenging. Thus, rational design of effective approaches to highly luminescent AuNCs, screening appropriate ligands for stabilizing AuNCs, evaluation of their biological toxicity and the availability for their surface modification, as well as figuring out their pathways and performances *in vivo* were all needed to be systematically studied. Most importantly, the improvement of the performances of AuNCs through active-targeted mode rather than passive-targeted mode should be further figured out.[28-37]

Controlled synthesis of AuNCs with a specific number of gold atoms in size range from tens to hundreds can well tune their structures and thus the optical properties. For instance, using protein as templates, Au_8, Au_{13}, and Au_{25} have been synthesized by controlling the reaction conditions.[16,28,38] In recent years, Au_{20}NCs have attracted increasing attention and stood out from various types of AuNCs owing to the following reasons: (i) the Au_{20}NC is highly stable and chemically inert due to its tetrahedral (T_d) structure; (ii) the Au_{20}NC has an extremely large energy gap (1.77 eV) which is even larger than that of C_{60} (1.57 eV), and an electron affinity comparable with that of C_{60}; (iii) the Au_{20}NC may exhibit unique optical and catalytic properties which are determined by its unique structure.[39-43]

To date, most dedications are mainly focused on the theoretical calculations and related discussions, with few report about the synthesis of Au_{20}NCs experimentally. For instance, Wang and co-workers prepared $Au_{20}(PPh_3)_8$ clusters (Ph = phenyl) in the solution for the first time.[40] Jin *et. al* synthesized thiolate-protected Au_{20}NCs with a large energy gap of 2.1 eV.[42] Their syntheses are successful but it is still challenging to obtain Au_{20}NCs with high QY and good stability in aqueous solution (*e.g.*, toluene was used in both of the reports). In the present work, we successfully achieved the rapid synthesis of protein-stabilized Au_{20}NCs in aqueous solution within 1 h together with high fluorescence QY up to ~15% by manipulating reaction kinetics. Specifically, the reaction needs to be carried out in alkali solution at relatively high temperature for generating highly luminescent Au_{20}NCs (2.6 nm in size), which also have good stabilities in different kinds of biological media, under a wide range of pH, under long-time irradiation, and for long-time storage. More importantly, systematic investigations of the Au_{20}NCs *in vitro* and *in vivo* have also conducted, including the cytotoxicity assay, toxicity evaluation for small animals, receptors-mediated cell internalization and imaging, as well as active tumor-targeted imaging in mice. Our results demonstrate the excellent biocompatibility of the as-prepared Au_{20}NCs, and the uptake of receptor-functionalized Au_{20}NCs by both cancer cells and tumor-bearing nude mice can be significantly improved by receptor-mediated internalization compared with the passive mode.

2. Experimental section

2.1. Materials

Reagents including folic acid (FA), hyaluronic acid (HA), 1-ethyl-3-[3-dimethylaminopropyl] carbodiimide hydrochloride (EDC), and N-hydroxysuccinimide (NHS) were all obtained from Sigma-Aldrich (St. Louis, USA). Hydrogen tetrachloroaurate (III) hydrate ($HAuCl_4 \cdot 3H_2O$) was purchased from Sinopharm Chemical Reagent Co., Ltd (Shanghai, China). Albumin from bovine serum (BSA) was obtained from Dingguo Changsheng Biotechnology Co., Ltd (Beijing, China). Mili-Q purified water (18.2 MΩ·cm) was used throughout the experiments.

2.2. Apparatus

Fluorescence spectra were measured with an F-2500 fluorescence spectrophotometer (Hitachi, Japan). Absorption spectra were recorded by a 3600 UV-Vis-NIR spectrophotometer (Shimadzu, Japan). Transmission electron microscopy (TEM) and high-resolution TEM (HRTEM) images were obtained with a Tecnai G2 F20 S-TWIN microscopy (FEI, USA). Atomic force microscopy (AFM) images were obtained using a Vecco multimode Nanoscope TM scanning probe microsystem (Vecco, USA). The conformation of proteins was recorded by a J-810 circular dichroism (CD) spectropolarimeter (Jacso, Japan). An FTIR-8400S Fourier transform infrared (FT-IR) spectrophotometer (Shimadzu, Japan) was employed to measure the IR spectra. X-ray photoelectron spectroscopy (XPS) analysis was conducted by an ESCALAB 250 X-ray photoelectron spectrometer (Thermo, USA). The molecular weights of BSA and BSA-AuNCs were analyzed by MALDI-TOF mass spectrometry on an AXIMA Performance (Shimadzu, Japan). The cellular fluorescence images were recorded by an IX81 microscope with a 40× objective (Olympus, Japan). The *in vivo* and *ex vivo* fluorescence imaging were performed by an In-Vivo FXPRO system (Caresteam Molecular Imaging, USA).

2.3. Synthesis of Au_{20}NCs

In a typical synthesis, an aqueous solution containing 5.8 mM of $HAuCl_4$ and 19.2 mg/mL of BSA was under vigorous magnetic stirring for 2 min. Then, NaOH (38 mM) was introduced to adjust the pH to 10. This mixture was allowed to incubate at 100 ^oC for 1 h. After the solution has been cooled to room temperature, the product could be collected by vacuum freeze-drying.

2.4. Conjugation of Au_{20}NCs with FA and HA

Preparation of FA-Au_{20}NC Conjugates. FA could be functionalized on the Au_{20}NCs by the conjugation of the amino groups of BSA and the carboxyls of FA using EDC/NHS. Typically, 25 mg of EDC and 15 mg of NHS were added to 1 mL of PBS buffer (pH 7.4) containing 10 mg of FA. The mixture was treated by sonication in dark at room temperature for 15 min, and then mixed with 2 mL of aqueous solution containing 200 mg of the Au_{20}NCs. This solution was allowed to react under magnetic stirring for 4 h. Afterwards, the pH of the solution was adjusted to 9, and the product was desalted and purified using a PD-10 Column.[28,31] Successful conjugation of FA with Au_{20}NCs was confirmed by FT-IR, UV-vis, CD, and fluorescence spectroscopy.

Preparation of HA-Au_{20}NC Conjugates. The protocol for the conjugation of Au_{20}NCs with HA is essentially the same as the

method for preparing FA-Au_{20}NC conjugates, except for the amount of reagents used. Specifically, 50 mg of EDC, 30 mg of NHS, 6.8 mg of HA, and 200 mg of Au_{20}NCs were introduced. The mixture was allowed to incubate for 8h.[44]

2.5. Toxicity Evaluation *in vitro* and *in vivo*

CCK-8 method was used to evaluate the cell viability in the presence of Au_{20}NCs and their conjugations,[28,31] where A549 and Hep-2 cancer cells were tested, respectively. In detail, the cells were plated in 96-well plates and subsequently incubated with Au_{20}NCs, FA-Au_{20}NCs, and HA-Au_{20}NCs, respectively, at 37 ^{o}C for 24 h. The concentrations of these probes were tested in the range of 20-100 mg/mL, and each concentration was tested with 3 sets of parallel samples. After 24 h incubation, each well was washed with PBS buffer for 3 times. Then, CCK-8 regent was added and incubated with the cells for 1 h at 37 ^{o}C. The optical density (OD) was measured at 450 nm with a multi-well plate reader, and the livability of cells could be calculated according to the OD values. A set of samples without the addition of the probes was also conducted as the control group.

The animal studies were carried out with the approval from the Ethics Committee of Southwest University and in compliance with the Principles of Laboratory Animal Care of the National Institutes of Health, China (No.: SYXK-2009-0002, Chongqing). For the *in vivo* toxicity studies, nude mice were used to test their weight changes in 4 weeks after the Au_{20}NCs, FA-Au_{20}NCs, and HA-Au_{20}NCs had been injected, respectively. The weights of these mice were recorded every week. The mice injected with the same volume of PBS were used as a control group. Error bars were obtained from three parallel experiments.

2.6. *in vitro* Targeted Fluorescence Imaging

Typically, Hep-2 and A549 cells were cleaved by trypsin, seeded, and grown onto 18 mm glass coverslips in a 24-well culture plate for 24 h. Then, an appropriate amount of Au_{20}NCs, FA-Au_{20}NCs, and HA-Au_{20}NCs were introduced and incubated for 4 h, respectively. The cells were washed thrice in PBS, fixed with 4% *p*-formaldehyde for 30 min, and mounted on microscope slides for fluorescence imaging.

2.7. Modeling Tumors in Mice and *in vivo* Tumor-Targeted Imaging

The athymic BALB/c (BALB/c-nu) mice (aged 3-4 weeks, weighed 18-20 g, equal number of male and female subjects) were obtained from Shanghai SLAC Laboratory Animal Co., Ltd. The tumor model was established by subcutaneous injection of HeLa, Hep-2, and A549 cancer cells (~10^7 in 200 μL of PBS) into the athymic nude mice, respectively. We obtained the *in vivo* fluorescent images at different time points after the probes were injected *via* tail vein, with the excitation and emission wavelengths of 470 nm and 600 nm, respectively. The *ex vivo* fluorescence images were captured immediately after the major organs/tumors were excised from the tested mice. Maestro Image software was employed to analysis the fluorescent intensity of the regions of interest (ROI) on the images.

3. Results and discussion

3.1. Rapid Synthesis and Characterization of the Protein-Stabilized Au_{20}NCs

For a typical synthesis, an aqueous solution containing $HAuCl_4$, BSA, and NaOH was incubated at 100 ^{o}C, and a reddish-brown solution containing AuNCs could be obtained after 1 h. Here, BSA acted as both a reductant and a stabilizer. NaOH was used to increase the pH value of the reaction solution (pH ≥ 10) to improve the reducing power of BSA and thus accelerate the reduction of Au^{3+} into Au^0.[14-16] Otherwise, AuNCs could not be obtained without the addition of any one of these reagents (SI, Figure S1). During the nucleation and growth processes, BSA also played an important role in restricting the size of the AuNCs.[14-16] In addition, the amount of reactants, temperature, and reaction time were also significant for obtaining the product with long wavelength emission and high QY (SI, Tables S1-4). As a result, a robust, readily, and reproducible protocol can be established for the synthesis of AuNCs (SI, Figure S2).

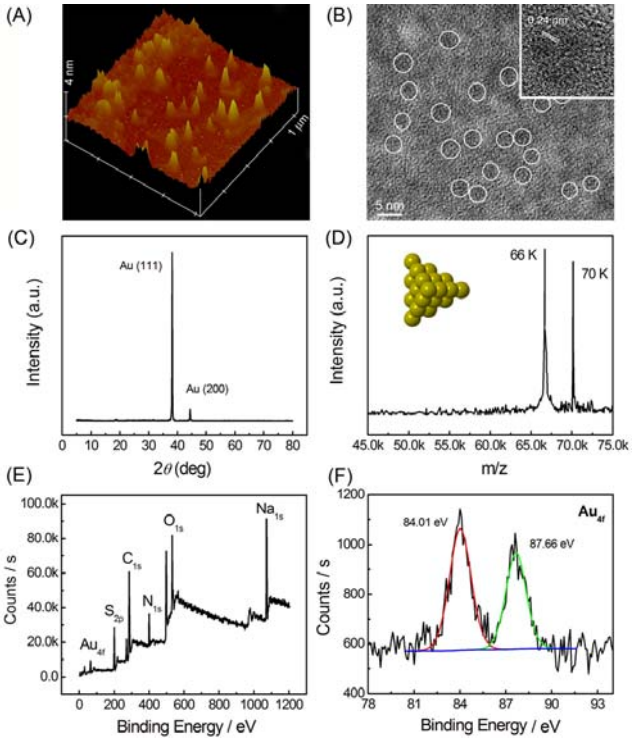

Figure 1 Characterization of the as-obtained protein-stabilized Au_{20}NCs: (A) AFM image of the Au_{20}NCs; (B) TEM and HRTEM (inset) images of the Au_{20}NCs; (C) XRD pattern of the Au_{20}NCs powder processed by freeze drying; (D) MALDI-TOF mass spectrum of the Au_{20}NCs; (E) XPS spectrum showing the binding energy of all elements of the product; (F) XPS spectrum showing the binding energy of Au_{4f}. The inset of (D) is the atomic model of Au_{20}NCs along <111> zone axis.

From the viewpoint of nucleation and growth, the concentration of Au atoms would steadily increase with the increase of reaction time, in which Au precursor could be depleted and reduced when a reductant (*i.e.*, BSA) was introduced. Once the concentration of Au atoms had reached the level of supersaturation, the atoms would start to aggregate into AuNCs through homogeneous nucleation.[45] Thus, the reaction kinetics should be crucial for controlling the number of Au atoms in a cluster and thus achieve high fluorescence QY. Previous studies on the synthesis of metal nanocrystals have demonstrated

that nucleation burst in relatively short period of time (*i.e.*, fast reaction rate) is conducive to generate a large number of clusters (or nuclei) and thus to obtain nanocrystals with relatively small sizes.[46-48] Here, in order to obtain subnanometer AuNCs, a fast reaction rate should be achieved to deplete essentially all the precursor in a short time period and thus restrict the growth of AuNCs into nanoparticles *via* heterogeneous nucleation. We found that the reaction rate could be speeded up by conducting the synthesis at relatively high temperature (*i.e.*, 100 ^{o}C) and under strong alkaline condition (*i.e.*, in the presence of 38 mM of NaOH). As a result, Au^{3+} was able to be converted into Au^{0} in a short period of time (less than 1 h) and formed the AuNCs. On the other hand, owing to the strong binding of amino acid residues (*e.g.*, cysteine) with the Au surface (or Au ions), BSA could act as a capping agent to minimize the surface free energy of the AuNCs,[45,49] and also a template to restrict further growth of the AuNCs into relatively larger Au nanoparticles.

To elucidate the morphology, structure, and composition of the as-prepared AuNCs, a series of characterizations were conducted. AFM images indicated that the average size of the AuNCs was ~2.6 nm (Figures 1A and S3), and the TEM image also confirmed their uniform sizes of 2~3 nm (Figure 1B). HRTEM image of a single AuNC (inset of Figure 1B) demonstrated the crystallinity of the face-centered cubic (*fcc*) Au. The lattice fringe spacing of 0.24 nm marked on its surface could be indexed to the {111} reflection of *fcc* Au. In addition, XRD pattern of the AuNCs power clearly displayed two peaks at $2\theta =$ 38.2^{o} and 44.4^{o} (Figure 1C), corresponding to diffractions from (111) and (200) lattice planes of Au, respectively (JCPDS 04-0784). The relatively stronger (111) diffraction peak than (200) peak indicated that the AuNCs were mainly covered by the low-energy {111} facets, and thus more (111) planes were oriented parallel to the flat surface of the supporting substrate.

MALDI-TOF mass spectrometric measurements showed two strong peaks at 66 and 70 kDa (Figure 1D). The peak at ~66 kDa was assigned to BSA, while the one at 70 kDa was assigned to the as-prepared BAS-AuNCs complex. That is, the peak shift of ~4 kDa relative to pure BSA indicated the formation of Au_{20}NCs in the BSA matrix. It has been demonstrated theoretically and experimentally that the Au_{20}NCs have a favorable structure of tetrahedron (T_d), which covered by four basic low-energy facets, {111}, of *fcc* Au.[39-43] As such, the Au_{20}NCs can be highly stable and chemically inert for various applications. Moreover, three different kinds of atoms in the *Td* structure, 4 at the apexes, 4 at the center of each face, and 12 along the edges (as shown in the inset of Figure 1D, atomic model), have different coordination environments and may provide ideal surface sites to bind different molecules. XPS spectrum of the BSA-stabilized Au_{20}NCs shows the binding energies of all the elements in the product (Figure 1E). Specifically, the elements of C, N, O, S, and Na were derived from the BSA and NaOH. The binding energies of 84.01 and 87.66 eV were corresponded to the zero-valence Au $4f_{7/2}$ and Au $4f_{5/2}$, respectively (Figure 1F). The spectrum of S 2p indicated the interaction of Au_{20}NCs with BSA through Au-S bond (SI, Figure S4). The result of thermal gravimetric analysis (TGA) indicated that the as-prepared Au_{20}NCs also had good thermal stability, with a weight loss of only ~10% even when the temperature reached 230 ^{o}C (SI, Figure S5). In addition, circular dichroism (CD) spectra showed that the two peaks at 208 and 220 nm, corresponding to the characteristic of alpha-helix of BSA, dramatically decreased and shifted to 204 nm and 226 nm, respectively (SI, Figure S6). It indicated that the conformation of the BSA had been changed after the formation of BSA-Au_{20}NCs complex. Combined all the results of the characterizations, it can be concluded that the protein-stabilized Au_{20}NCs with uniform and small sizes could be readily obtained using the present protocol.

3.2. Fluorescence and Stability of the Au_{20}NCs

As shown in Figure 2A, the as-obtained Au_{20}NCs were highly dispersed in aqueous solution and exhibited strong red fluorescence under a UV lamp (λ_{ex} = 365 nm). The maximal excitation and emission peaks were located at 470 and 620 nm, respectively. We further prepared an Au_{20}NCs-agar gel by mixing a certain concentration of Au_{20}NCs with 5% (w/v) agar at relatively high temperature, which also exhibited strong red fluorescence under a UV light after the mixture had been cooled to room temperature. This result demonstrated that the Au_{20}NCs could be a promising candidate for making solid fluorescent substrates or devices.

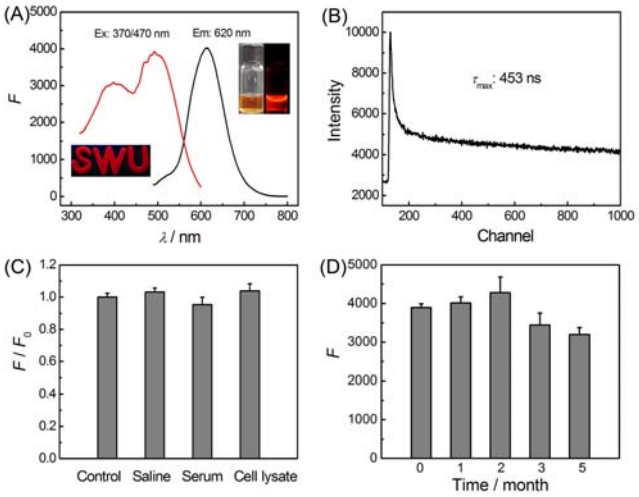

Figure 2 Photoluminescence of Au_{20}NCs prepared in the present work. (A) Excitation and emission spectra of the Au_{20}NCs. The insets show the digital photos of the Au_{20}NCs solution (right) and solid Au_{20}NCs-agar gel under UV light (365 nm), respectively; (B) Fluorescence decay curve of the Au_{20}NCs; (C) Fluorescence stability of the Au_{20}NCs in different physiological media. Saline was an aqueous solution containing 0.9% NaCl (w/v), and the concentrations of serum and cell lysate were 10% and 20% (w/v), respectively; (d) Fluorescence intensity changes of the as-prepared Au_{20}NCs within 5 months.

Under optimal conditions, Au_{20}NCs with high fluorescent QY (14.8 ± 2.2%, measured with fluorescein as a reference dye; 14.5 ± 2.0%, measured by Quantaurus-QY which can obtain the QY without any reference) could be obtained. To our knowledge, these QY values are obviously higher than those of most previously prepared AuNCs which are usually lower than 6% (SI, Table S5). The relaxation time for the fluorescence decay of the Au_{20}NCs (Figure 2B, Table S6) was much longer than that in previous report, in which BSA was used for the synthesis at 37

^{o}C (lifetime: 453 *vs*. 184 ns).[28,38] It is obviously that the relatively long lifetime of the as-prepared Au_{20}NCs can take advantages in the optical-related applications such as biolabeling, biosensing, and bioimaging, especially for *in vivo* studies.

The Au_{20}NCs also showed good stabilities when they were dispersed in various media such as physiological saline (0.9% NaCl aqueous solution), 10% serum, 20% cell lysate, and aqueous solution in a wide pH range of 2-10 (Figures 2C and S7-9). Photobleaching was not observed even if they had been continuously irradiated with UV light for 60 min (Figure S10). Moreover, the Au_{20}NCs could be used and stored for 5 months (Figure 2D). Taking together, we can conclude that the as-prepared Au_{20}NCs have high stabilities in different media, under different pH, under long time irradiation, and also can be used or stored in a long period of time. Such ideal stability may be attributed to the unique *Td* structure of the Au_{20}NCs and the strong binding between protein template and Au species. Furthermore, the surfaces of Au_{20}NCs can be easily modified with a variety of probe molecules owing to rich functional groups in BSA template, making them effectively across the biological barriers and thus readily achieve the bioimaging.

3.3. Receptor-Mediated Cell Internalization and Imaging *in vitro*

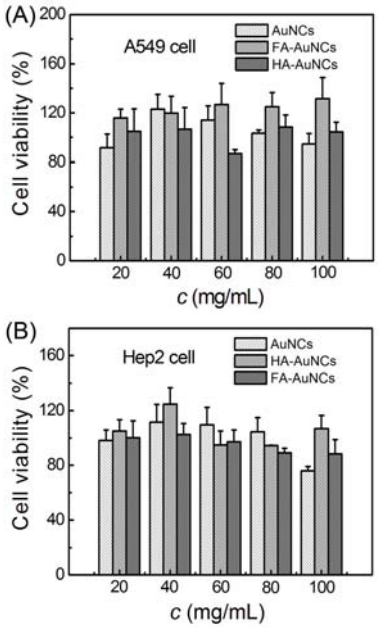

Figure 3 The viabilities of cells after incubated with different dosages of Au_{20}NCs, FA-Au_{20}NCs, and HA-Au_{20}NCs *in vitro* for 24 h, respectively. Two kinds of cancer cells were tested for studying the toxicity of the as-prepared materials against the cells: (A) A549 cell, and (B) Hep-2 cell. All the data were obtained by conducting three parallel experiments.

Benefiting from the advantages of high fluorescence QY, small sizes, and good stability, the as-prepared Au_{20}NCs can be ideal candidates for optical and biological applications. Thus, the Au_{20}NCs with different concentrations were tested as fluorescent probes for cell imaging. It was found that the fluorescence emission in cells could be clearly observed only when more than 10 mg/mL of Au_{20}NCs were incubated with the cells (SI, Figure S11), revealed the limitation of the uptake of Au_{20}NCs *via* endocytosis (*i.e.*, passive targeting). In contrast, we believe the receptor-mediated endocytosis (*i.e*., active targeting) will be a more efficient pathway for cell imaging, using multi-functionalized probes containing both signal reporters and recognition components. To this end, together with the strong fluorescence signal, we further functionalized the Au_{20}NCs with folic acid (FA) and hyaluronic acid (HA) as a recognition component for active tumor-targeted imaging, respectively. The mixture of EDC and NHS were used to cross-link the BSA-Au_{20}NCs with FA and HA, respectively. UV-Vis, IR, and CD spectra all indicated the cross-linking was achieved, and the fluorescence properties of the Au_{20}NCs were not changed after the cross-linking (SI, Figures S12, S13).

Cytotoxicity evaluation demonstrated the Au_{20}NCs and their functionalized conjugates (FA-Au_{20}NCs and HA-Au_{20}NCs) all had good biocompatibility. As shown in Figure 3, the viabilities of both A549 and Hep-2 cells maintained above 90% when they had been incubated with Au_{20}NCs, FA-Au_{20}NCs, and HA-Au_{20}NCs in the concentration range of 20-100 mg/mL for 24 h, respectively. As such, these two kinds of functionalized Au_{20}NCs, FA-Au_{20}NCs and HA-Au_{20}NCs, were further employed as optical probes for active targeting imaging of cancer cells *in vitro*, respectively. FA is a widely used recognition component for targeting cancer cells, because FA receptor can be over-expressed on the surfaces of many kinds of cancer cells while be highly restricted in normal tissues.[50] Thus, the FA-mediated endocytosis is highly effective for active tumor-targeting and thus distinguishing the cancer and normal tissues. Hep-2 cancer cells, which can over-express FA receptor, were used herein to test the targeting specificity of the FA-Au_{20}NCs.

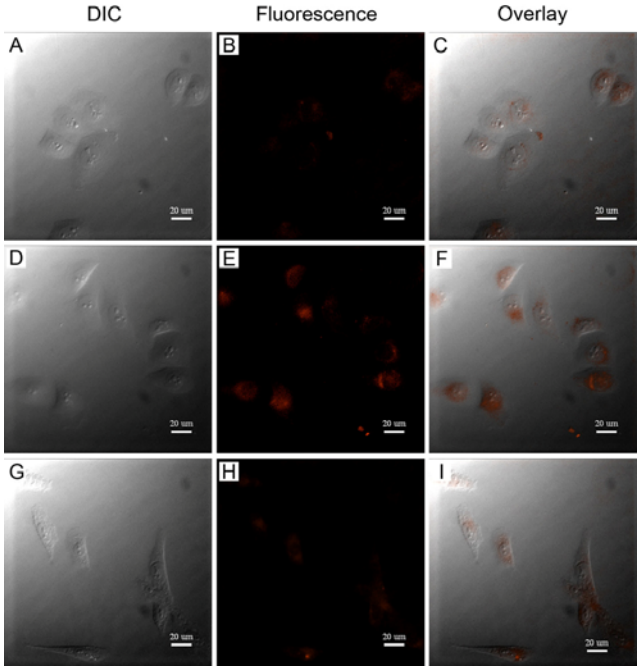

Figure 4 Fluorescence imaging showing the delivery of (A-C) Au_{20}NCs and (D-F) functionalized FA-Au_{20}NCs into the living Hep-2 cells. The images of (G-I) show the delivery of functionalized FA-Au_{20}NCs into the living A549 cells which can only express low amount of FA receptor (a negative control group). The images of differential interference contrast (DIC) (A, D, G), fluorescence (B, E, H), and the overlay of DIC and fluorescence mode (C, F, I) were all recorded. Au_{20}NCs and FA-Au_{20}NCs

with the concentration of 6 mg/mL were used. Scale bars, 20 μm.

As shown in Figure 4, strong red fluorescence could be clearly observed in the Hep-2 cells after they had been incubated with FA-Au_{20}NCs for 4 h (Figure 4 D-F), while very weak fluorescence was observed when pure Au_{20}NCs was introduced (Figure 4 A-C). The dramatic difference demonstrated that the active targeting could indeed improve the uptake of Au_{20}NCs into cancer cells. In another set of control experiment, A549 cancer cells which can only express low amount of FA receptor were used for comparison. Like the result from pure Au_{20}NCs, only weak fluorescence was observed (Figure 4 G-I), confirming that the FA receptor plays a critical role in active targeted imaging.

Except for the FA-Au_{20}NCs, cell internalization of HA-Au_{20}NCs was also studied to verify the universality of the functionalized Au_{20}NCs for receptor-mediated active targeted imaging. HA, a kind of glycosaminoglycan, can selectively bind with receptor CD44, which is also a well-known marker for cancer cells.[44] A549 cells, which can over-express CD44 and thus can selectively bind to HA-based conjugates with high affinity, were used herein. As shown in Figure 5, very weak fluorescence was observed when a mix of 6 mg/mL pure Au_{20}NCs and a certain concentration of free HA (control group) had been incubated with the A549 cells (Figure 5 A-C). In contrast, relatively strong fluorescence could be observed when the same concentration of HA-Au_{20}NCs was introduced (Figure 5 D-F). Obviously, the improved uptake of Au_{20}NCs by A549 cells relative to the control group was attributed to the CD44-mediated cell internalization. These two successful *in vitro* demonstrations suggest that the functionalized Au_{20}NCs are promising candidates for active tumor-targeted imaging and thus can be potentially applied in cancer diagnosis.

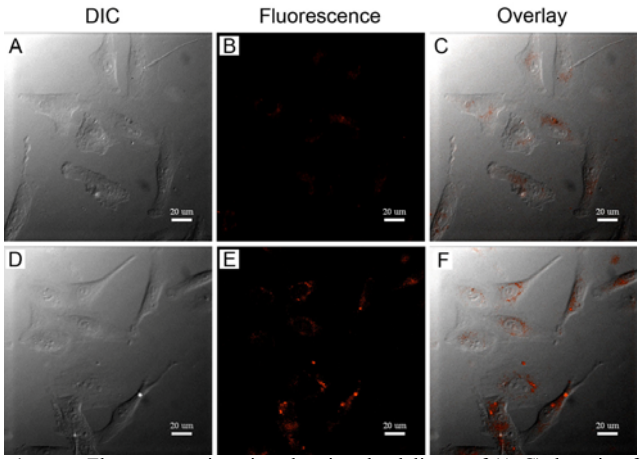

Figure 5 Fluorescence imaging showing the delivery of (A-C) the mix of Au_{20}NCs and free HA and (D-F) functionalized HA-Au_{20}NCs into the living A549 cells. The images of differential interference contrast (DIC) (A and D), fluorescence (B and E), and the overlay of DIC and fluorescence mode (C and F) were all recorded. Au_{20}NCs and HA-Au_{20}NCs with the concentration of 6 mg/mL were used. Scale bars, 20 μm.

3.4. Active Tumor-Targeted Imaging *in vivo*

To evaluate the toxicity of Au_{20}NCs and functionalized Au_{20}NCs *in vivo*, we further monitored the body weights of mice in 4 weeks after they had been injected with these probes. The weights of the nude mice in control group (injected with the same volume of PBS buffer) were slightly increased from ~18 to ~21 g in 4 weeks owing to the normal growth (Figure S14). Like the control group, the mice injected with the fluorescent probes, regardless of tumor-bearing or not, showed similar tendency in body weight changes. In addition, no diarrhoea and other signs of acute toxicological response as well as long toxic effects were observed for all the mice. The results demonstrated non-toxic nature of the Au_{20}NCs and their conjugates. Therefore, it can be concluded that the Au_{20}NCs-based materials can be excellent candidates for *in vivo* applications.

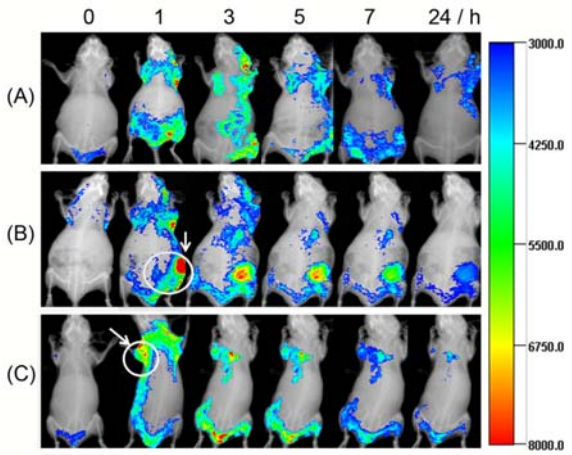

Figure 6 Time-dependent distributions of FA-Au_{20}NCs in (A) normal nude mice, (B) HeLa tumor-bearing nude mice, and (C) A549 tumor-bearing nude mice, which were monitored by an NIR fluorescence imaging system. For each set of experiment, 200 μL of 60 mg/mL FA-Au_{20}NCs were injected into the mice through tail vein. The locations of the tumor were marked by white arrows.

We further employed the functionalized Au_{20}NCs for active tumor-targeted imaging *in vivo*. Two kinds of mice, modeling with HeLa and A549 tumors, were tested for the active targeting using FA-Au_{20}NCs as fluorescent probes. Ideally, HeLa cells can over-express FA receptor and thus can facilitate the uptake of FA-Au_{20}NCs, whereas A549 cells can only express low amount of FA receptor (a negative control group for comparison).[28,31,50] As shown in Figure 6 A, the FA-Au_{20}NCs distributed almost all over the body of normal mice (without tumor) at the initial stage (0-3 h), and subsequently were metabolized and cleared over the time through the hepatic and renal pathways. However, the strong fluorescence derived from the FA-Au_{20}NCs dramatically appeared at the location of HeLa tumor (as marked by white arrow) at 1 h after injection, and it was much stronger than the other parts of the mice (Figure 6 B). The fluorescence at the tumor site could be maintained for a relatively long time (~72 h), while the fluorescence at other sites of the mice gradually decreased as the time increased (the picture of the HeLa tumor-bearing mouse is shown in Figure S15A). When the mice were switched to the ones bearing A549 tumor, although the fluorescence at the tumor site was relatively stronger than other sites (Figure 6 C), it was still much weaker relative to the fluorescence at the HeLa tumor as shown in Figure 6 B. This result indicated that the uptake of large amount of FA-Au_{20}NCs by HeLa tumor could be readily achieved through receptor-mediated active targeting, while only a few amount of the FA-

Au_{20}NCs could be taken into the A549 tumor *via* enhanced permeability and retention (EPR) effect. The EPR effect was also confirmed by comparing the fluorescence response as a function of time between the normal mice and the Hep-2 tumor-bearing mice with the injection of pure Au_{20}NCs (SI, Figure S16). Combined together, it is obvious that the functionalized Au_{20}NCs could be accumulated at the tumor sites with a relatively high concentration through active tumor-targeted endocytosis.

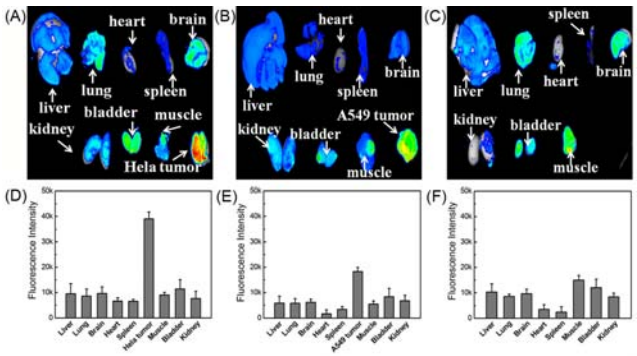

Figure 7 *Ex vivo* (A-C) fluorescence images and (D-F) average fluorescence intensity analysis of the tumor tissue and major organs of the mice, which were sacrificed at 7 h after the injection of the FA-Au_{20}NCs (200 μL, 60 mg/mL): (A) the mice bearing HeLa tumor; (B) the mice bearing A549 tumor; (C) normal mice; (D-F) statistical analysis of the fluorescence intensity corresponded to the *ex vivo* fluorescence images of (A-C).

The *ex vivo* fluorescence images of various tissues were also obtained *via* thoracotomy, which were performed at 7 h post-injection of the FA-Au_{20}NCs. Representative tissues including tumor, heart, liver, spleen, lung, kidney, brain, bladder, and muscle around the tumor were excised, washed with PBS buffer, and then used for fluorescence imaging. The corresponding regions of interest (ROI) analysis on the *ex vivo* fluorescence images was conducted to semi-quantitatively study the uptake of FA-Au_{20}NCs in each organ by the Maestro software. As shown in Figure 7, the *ex vivo* HeLa tumor showed much stronger fluorescence than other organs, and its average ROI fluorescence intensity was at least 4.5 times higher than that of other organs (Figure 7A, D). In comparison, relatively weak fluorescence was observed at the A549 tumor (~2 times higher than other organs, Figure 7B, E) since very limited FA receptor can be expressed on the surface of A549 cells. The results from the *ex vivo* imaging and ROI assay were consistent with the observations from the *in vivo* fluorescence imaging. In addition, we found that the probes tended to accumulate in tumor, kidney, and bladder, indicating that the FA-Au_{20}NCs are promising candidates for noninvasive real-time imaging *in vivo* and also can be removed from the body through renal clearance.

To confirm the universality of the functionalized Au_{20}NCs as probes for active tumor-targeted imaging, HA-Au_{20}NCs were further tested *in vivo* in the same way. In this set of experiment, Hep-2 tumor was employed as a typical model to test the CD44-mediated internalization since Hep-2 cells could over-express CD44 for recognizing HA (the picture of the Hep-2 tumor-bearing mouse is shown in Figure S15B). As shown in Figure 8A, strong fluorescence of HA-Au_{20}NCs dramatically appeared at the Hep-2 tumor site (as marked by white arrow) at 1 h after injection, and it was also much stronger than the other sites of the mice. Like the evolution of FA-Au_{20}NCs in HeLa tumor, the fluorescence of HA-Au_{20}NCs could also be maintained at the tumor sites for a relatively long time. For the negative control group (injecting HA-Au_{20}NCs into normal mice), the fluorescent probes were distributed all over the body (Figure 8B). Compared with the case as shown in Figure 8A, the Hep-2 tumor-bearing mice injected by a mix of the same amount of free Au_{20}NCs and HA showed much weaker fluorescence at the tumor site (Figure 8C), demonstrating the importance of conjugation of Au_{20}NCs with HA. The *ex vivo* fluorescence imaging and ROI assay indicated that the average fluorescence intensity of the Hep-2 tumor was about 6 times higher than that of other tissues (Figure 9A, D). However, the intensity of the probes entered into the tumor through EPR effect was much lower (~3 times higher than other organs) (Figure 9B, E). This remarkable difference further demonstrated that the uptake of nanoprobes into the tumor sites could be improved by receptor-mediated internalization rather than by passive targeting.

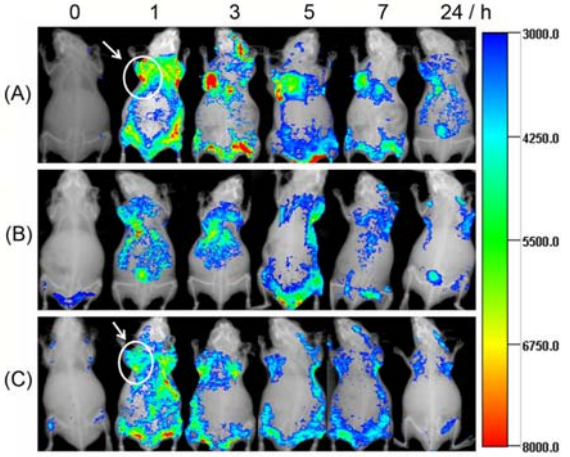

Figure 8 Time-dependent distributions of HA-Au_{20}NCs in (A) Hep-2 tumor-bearing nude mice and (B) normal nude mice, which were monitored by an NIR fluorescence imaging system. For each set of experiment, 200 μL of 60 mg/mL HA-Au_{20}NCs were injected into the nude mice through tail vein. (C) Time-dependent fluorescence images of the Hep-2 tumor-bearing mice after injected with a mix of the same amount of Au_{20}NCs and free HA. The locations of the tumor were marked by white arrows.

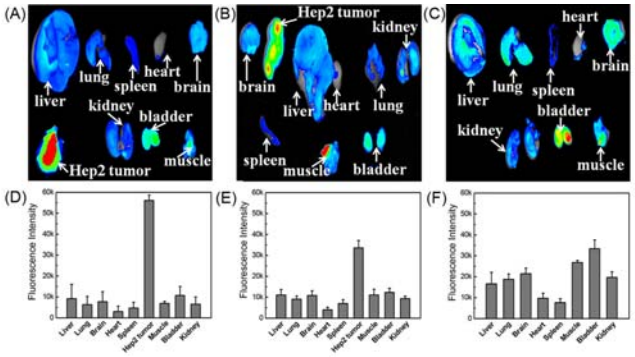

Figure 9 *Ex vivo* (A-C) fluorescence images and (D-F) average fluorescence intensity analysis of the tumor tissue and major organs of the mice, which were sacrificed at 7 h after the injection of the fluorescent probes: (A) the mice bearing Hep-2 tumor injected with HA-Au_{20}NCs; (B) the mice bearing Hep-2 tumor injected with a mix of Au_{20}NCs and free HA; (C) normal mice injected with HA-Au_{20}NCs; (D-F)

statistical analysis of the fluorescence intensity corresponded to the *ex vivo* fluorescence images of (A-C).

It can be concluded that the distinguishable fluorescence between the tumor sites and the body background is attributed to the following reasons: (i) the receptor-mediated specific endocytosis can selectively recognize, deliver, and accumulate the functionalized Au_{20}NCs to the tumor sites, resulting in the strong fluorescence at these sites; (ii) the Au_{20}NCs with such small sizes can largely avoid the uptake by reticuloendothelial system and thus readily reach the tumor sites through EPR effect or active targeting; (iii) the as-prepared Au_{20}NCs with strong fluorescence emission at relatively long wavelength can make the imaging avoid the interference of the auto-fluorescence from the organism.

4. Conclusions

We successfully achieved the rapid synthesis of protein-stabilized Au_{20}NCs within 1 h together with high fluorescence QY up to ~15%. We found that highly luminescent Au_{20}NCs could be obtained by manipulating the reaction kinetics at an appropriate temperature and using a certain amount of alkali. Structural and morphological characterizations demonstrated the uniform size of ~2.6 nm of the Au_{20}NCs. Taking their advantages of small size, good stability in biological media, strong fluorescence emission, excellent photostability, and non-toxicity, Au_{20}NCs and the corresponding functionalized conjugates were further used as fluorescent probes for biological imaging *in vitro* and *in vivo*.

Our results demonstrated that the uptake of functionalized Au_{20}NCs by cancer cells and tumor-bearing nude mice could be greatly improved by active-targeted mode (namely, receptor-mediated internalization) compared to the passive-targeted mode. The relatively strong fluorescence observed at the tumor sites derived from the selectively accumulated Au_{20}NCs allowed the as-prepared probe to be a potential indicator for the cancer diagnosis. This work represents a systemic investigation of the Au_{20}NCs from synthesis to characterization, from *in vitro* to *in vivo* imaging, and from microcosmic- to macroscopic-scale applications. We believe this general strategy for active tumor-targeted optical imaging based on the functionalized Au_{20}NCs is promising to be applied in clinical cancer diagnosis and therapy.

Acknowledgements

This work was supported by the National Natural Science Foundation of China (NSFC, No. 21035005).

Notes and references

[a] *Education Ministry Key Laboratory on Luminescence and Real-Time Analysis, College of Pharmaceutical Sciences, Southwest University, Chongqing 400715, China. E-mail: chengzhi@swu.edu.cn, Tel: (+86) 23 68254659, Fax: (+86) 23 68367257.*
[b] *School of Chemistry and Chemical Engineering, Southwest University, Chongqing 400715, China.*
[c] *School of Physical Science and Technology, Southwest University, Chongqing 400715, China;*
[d] *Life Science & Clinical Medicine Department, Shimadzu (China) Co., Shanghai 200052, China.*

† Electronic Supplementary Information (ESI) available: Additional Figures and Tables. See DOI: 10.1039/b000000x/

1. Y. Yang, Q. Zhao, W. Feng, F. Li, *Chem. Rev.*, 2013, **113**, 192-270.
2. C.-H. Quek, K. W. Leong, *Nanomaterials*, 2012, **2**, 92-112.
3. S. Kunjachan, F. Gremse, B. Theek, P. Koczera, R. Pola, M. Pechar, T. Etrych, K. Ulbrich, G. Storm, F. Kiessling, T. Lammers, *ACS Nano*, 2013, **7**, 252-262.
4. J. Lovell, T. Liu, J. Chen, G. Zheng, *Chem. Rev*., 2010, **110**, 2839-2857.
5. D. M. Shcherbakova, O. M. Subach, V. V. Verkhusha, *Angew. Chem. Int. Ed*., 2012, **51**, 10724-10738.
6. H. Shi, X. He, K. Wang, X. Wu, X. Ye, Q. Guo, W. Tan, Z. Qing, X. Yang, B. Zhou, *Proc. Natl. Acad. Sci. USA.*, 2011, **108**, 3900-3905.
7. H. M. Kim, H. Lee, K. Hong, M. Y. Cho, M.-H. Sung, H. Poo, Y. T. Lim, *ACS Nano*, 2011, **5**, 8230-8240.
8. C.-Y. Zhang, H.-C. Yeh, M. T. Kuroki, T.-H. Wang, *Nat. Mater.*, 2005, **4**, 826-831.
9. L. Q. Chen, S. J. Xiao, P. P. Hu, L. Peng, J. Ma, L. F. Luo, Y. F. Li, C. Z. Huang, *Anal. Chem*., 2012, **84**, 3099-3110.
10. X. Huang, F. Zhang, L. Zhu, K. Y. Choi, N. Guo, J. Guo, K. Tackett, P. Anilkumar, G. Liu, Q. Quan, H. S. Choi, G. Niu, Y.-P. Sun, S. Lee, X. Chen, *ACS Nano*, 2013, **7**, 5684-5693.
11. X. Xu, Y. Chen, H. Wei, B. Xia, F. Liu, N. Li, *Anal. Chem*., 2012, **84**, 9721-9728.
12. L. A. Peyser, A. E. Vinson, A. P. Bartko, R. M. Dickson, *Science*, 2001, **291**, 103-106.
13. H. Xu, K. S. Suslick, *Adv. Mater*., 2010, **22**, 1078-1082.
14. L. Shang, G. U. Nienhaus, *Biophys Rev*., 2012, **4**, 313-322.
15. D. M. Chevrier, A. Chatt, P. Zhang, *J. Nanophoton*., 2012, **6**, 064504.
16. J. Xie, Y. Zheng, J. Y. Ying, *J. Am. Chem.Soc*., 2009, **131**, 888-889.
17. H. Zhang, X. Huang, L. Li, G. Zhang, I. Hussain, Z. Li, B. Tan, *Chem. Commun*., 2012, **48**, 567-569.
18. X. Yuan, Z. Luo, Q. Zhang, X. Zhang, Y. Zheng, J. Y. Lee, J. Xie, *ACS Nano*, 2011, **5**, 8800-8808.
19. E. S. Shibu, B. Radha, P. K. Verma, P. Bhyrappa, G. U. Kulkarni, S. K. Pal, T. Pradeep, *ACS Appl. Mater. Interfaces*, 2009, **10**, 2199-2210.
20. C. Wang, Y. Wang, L. Xu, X. Shi, X. Li, X. Xu, H. Sun, B. Yang, Q. Lin, *Small*, 2013, **9**, 413-420.
21. M. L. Tran, A. V. Zvyagin, T. Plakhotnik, *Chem. Commun.*, 2006, 2400-2401.
22. K.-Y. Pu, Z. Luo, K. Li, J. Xie, B. Liu, *J. Phys. Chem. C*, 2011, **115**, 13069-13075.
23. Z. Wu, M. A. MacDonald, J. Chen, P. Zhang, R. Jin, *J. Am. Chem. Soc*., 2011, **133**, 9670-9673.
24. Z. Tang, T. Ahuja, S. Wang, G. Wang, *Nanoscale*, 2012, **4**, 4119-4124.
25. T. A. C. Kennedy, J. L. MacLean, J. Liu, *Chem. Commun.*, 2012, **48**, 6845-6847.
26. L. Fabris, S. Antonello, L. Armelao, R. L. Donkers, F. Polo, C. Toniolo, F. Maran, *J. Am. Chem. Soc.*, 2006, **128**, 326-336.
27. L. Yan, Yu. Cai, B. Zheng, H. Yuan, Y. Guo, D. Xiao, and M. M. F. Choi，*J. Mater. Chem.*, 2012, **22**, 1000-1005.
28. A. Retnakumari, S. Setua, D. Menon, P. Ravindran, H. Muhammed, T. Pradeep, S. Nair, M. Koyakutty, *Nanotechnology*, 2010, **21**, 55103-55115.
29. C.-L. Liu, H.-T. Wu, Y.-H. Hsiao, C.-W. Lai, C.-W. Shih, Y.-K. Peng, K.-C. Tang, H.-W. Chang, Y.-C. Chien, J.-K. Hsiao, J.-T. Cheng, P.-T. Chou, *Angew. Chem. Int. Ed.*, 2011, **50**, 7056-7060.
30. P. L. Xavier, K. Chaudhari, P. K. Verma, S. K. Pal, T. Pradeep, *Nanoscale*, 2010, **2**, 2769-2776.
31. H. Chen, S. Li, B. Li, X. Ren, S. Li, D. M. Mahounga, S. Cui, Y. Gu, S. Achilefu, *Nanoscale*, 2012, **4**, 6050-6064.
32. X. Wu, X. He, K. Wang, C. Xie, B. Zhou, Z. Qing, *Nanoscale*, 2010, **2**, 2244-2249.
33. J.-M. Liu, J.-T. Chen, X.-P. Yan, *Anal. Chem*., 2013, **85**, 3238-3245.
34. C. Sun, H. Yang, Y. Yuan, X. Tian, L. Wang, Y. Guo, L. Xu, J. Lei, N. Gao, G. J. Anderson, X.-J. Liang, C. Chen, Y. Zhao, G. Nie, *J. Am. Chem. Soc.*, 2011, **133**, 8617-8624.
35. Y. Wang, J.-T. Chen, X.-P. Yan, *Anal. Chem*., 2013, **85**, 2529-2535.
36 S.-K. Sun, L.-X. Dong, Y. Cao, H.-R. Sun, and X.-P. Yan, *Anal. Chem.*, 2013, **85**, 8436-8441.

37. D.-H. Hu, Z.-H. Sheng, P.-F. Zhang, D.-Z. Yang, S.-H. Liu, P. Gong, D.-Y. Gao, S.-T. Fang, Y.-F. Ma and L.-T. Cai, *Nanoscale*, 2013, **5**, 1624-1628.
38. X. L. Guevel, B. Hotzer, G. Jung, K. Hollemeyer, V. Trouillet, M. Schneider, *J. Phys. Chem. C*, 2011, **115**, 10955-10963.
39. J. Li, X. Li, H.-J. Zhai, L.-S. Wang, *Science*, 2003, **299**, 864-867.
40. H.-F. Zhang, M. Stender, R. Zhang, C. Wang, J. Li, L.-S. Wang, *J. Phys. Chem. B*, 2004, **108**, 12259-12263.
41. E. S. Kryachko, F. Remacle, *Int. J. Quantum Chem*., 2007, **107**, 2922-2934.
42. M. Zhu, H. Qian, R. Jin, *J. Am. Chem. Soc*., 2009, **131**, 7220-7221.
43. Z. W. Wang, R. E. Palmer, *Nanoscale*, 2012, **4**, 4947-4949.
44. E. J. Goh, K. S. Kim, Y. R. Kim, H. S. Jung, S. Beack, W. H. Kong, G. Scarcelli, S. H. Yun, S. K. Hahn, *Biomacromolecules*, 2012, **13**, 2554-2561.
45. Y. Xia, Y. Xiong, B. Lim, S. E. Skrabalak, *Angew. Chem. Int. Ed.*, 2009, **48**, 60-103.
46. A. R. Tao, S. Habas, P. Yang, *Small*, 2008, **4**, 310-325.
47. Y. Wang, Y. Zheng, C. Z. Huang, Y. Xia, *J. Am. Chem. Soc.*, 2013, **135**, 1941-1951.
48. Y. Wang, S.-I. Choi, X. Zhao, S. Xie, H.-C. Peng, M. Chi, C. Z. Huang, Y. Xia, *Adv. Funct. Mater.*, 2013, DOI: 10.1002/adfm.201302339.
49. Y. Xia, X. Xia, Y. Wang, S. Xie, *MRS Bull.*, 2013, **38**, 335-344.
50. N. Parker, M. J. Turk, E. Westrick, J. D. Lewis, P. S. Low, C. P. Leamon, *Anal. Biochem*., 2005, **338**, 284-293.